



# An Alternative Method for Stable Machining on a Small Workspace Mill-Turn Machine

Trung-Kien Vi<sup>1,4\*</sup>, Yung-Chou Kao<sup>2</sup>, Sheng-Jhe Chen<sup>2</sup>, Guo-Hua Feng<sup>3</sup> and Sung-Yan Tsai<sup>1</sup>

<sup>1</sup> Department of Mechanical Engineering, National Chung Cheng University, No. 168, Sec. 1, University Rd., Minhsiung Township, Chiayi County 621301, Taiwan (R.O.C.)

<sup>2</sup> Advanced Institute of Manufacturing with high-tech Innovations, National Chung Cheng University, No. 168, Sec. 1, University Rd., Minhsiung Township, Chiayi County 621301, Taiwan (R.O.C.)

<sup>3</sup> Department of Power Mechanical Engineering, National Tsing Hua University, No. 101, Section 2, Kuang-Fu Road, Hsinchu City 30013, Taiwan (R.O.C.)

<sup>4</sup> Faculty of Electromechanic and Electronics, Lac Hong University, No. 10, Huynh Van Nghe Street, Buu Long ward, Bien Hoa City, Dong Nai Province, Viet Nam.

\*Corresponding author: [vitrungkien@gmail.com](mailto:vitrungkien@gmail.com)

Received: 15<sup>th</sup> March 2022

Revised: 08<sup>th</sup> May 2022

Accepted: 24<sup>st</sup> June 2022

OPEN ACCESS 

**Abstract:** In theoretically traditional practice, the cutting force calculation/prediction based on the cutting force coefficients (CFCs) will not be affected by the properties of the machine tool such as the structural dynamics and the Frequency Response Function (FRF), etc. It means the CFCs are related only to the paired cutting tool and workpiece, but not the machine. However, it seems to be not the same in practice. This paper proposes an alternative method by conducting the cutting test experiment on the other machines that have enough working space for a dynamometer to be installed for the cutting test, and then applying it to a small working space machine. A series of experiments had been designed for cutting test and tapping test to verify the proposed method. This paper then focused on the exploration of varieties that influence the cutting forces. Finally, a new stable machining method has been successfully developed and verified with a case study by using a real seven-axis mill-turn machine tool (MTM) different from the machine tools used for the cutting test.

**Keywords:** Stability Lobe Diagram; Small-workspace Mill-Turn; Stable Machining; Cutting Force Coefficients

## Introduction

Machine tools encounter both forced and self-excited vibrations during machining operations. Prediction of the cutting forces has been studied over the years and it can help to avoid chatter, tool breakage, deformation, etc. Knowledge of cutting forces is very important because it leads to an efficient machining process through the proper selection of metal cutting parameters, machine tools, fixtures, and tools. The traditional mechanistic approach is frequently utilized in predicting the cutting forces, where the cutting force coefficients (CFC) are obtained through the experimental curve fitting to measured average cutting forces. Lee and Altintas [1] predicted cutting forces in ball-end milling from orthogonal cutting data and found that the predicted and simulated cutting forces in ball-end mill operations were in good agreement. Shirase and Altintas [2] studied cutting force and dimensional surface error generation in

peripheral milling with variable pitch helical end mill. The accuracy of the predicted milling forces for the helical end mill has been verified for several cutting tests. And the force prediction in variable pitch cutter was used to reduce dimensional surface errors as well as suppress chatter vibrations. Budak, Altintas, and Armarego [3] predicted milling force coefficients from orthogonal cutting data. The percentage deviations of the average and the maximum cutting force prediction from the measurements was about 81% of the force predictions; less than  $\pm 10\%$  deviation in the x and y directions and the maximum deviation in all cases is less than 25%. Altintas and Lee [4] developed a dynamic model for the helical end mill. They simulated and experimentally measured cutting force in three Cartesian directions and the results are similar to each other and in agreement with those obtained from over 130 end milling experiments at different cutting conditions and cutter geometry as reported by Budak et al [3]. A sample simulation and experimentally measured cutting force, are in good agreement even though the axial depth of cut and the chip thickness distribution is very small. Smith and Tlustý [5-6] modified their turning analysis and developed the SLD of helical endmills for milling. And they had shown that the analysis of the SLD is more important in high-speed milling because there is a wide and highly stable cutting area during high-speed milling. Their algorithm assumed an average angle of the tooth in the cut and average cutting force direction. The corresponding spectrum shows a dominant peak very close to the natural frequency of the system (383 Hz) and not at the tooth frequency (800 Hz). This confirms the experimental observation of chatter and verifies the onset of chatter predicted by the model. Altintas and Budak [7-8] developed an analytical solution to stability lobes in milling which accurately predicted the stability of slotting operation. Their method is similar to that of Tlustý mentioned above. However, they approximated the time-dependent cutting forces by average value but employed a different approach to identifying this mean and the development of the time-dependent cutting force equations. In the Fourier series solution, for this case, however, the single-frequency approximation, which provides a complete analytical solution without any iteration, is in excellent agreement with the time domain simulation and multi-frequency solution. Turner et al. [9] developed the SLD of the variable helix end mill. The stability lobe is computed with the time domain model using Cutpro™. Shamoto et al [10] developed the method for the analytical prediction of chatter stability in ball-end milling with tool inclination. The analytical and experimental results are all in good agreement. Besides, Wan et al [11] developed SLD for multiple delay milling

**Trung-Kien Vi** is currently pursuing a Ph.D. at National Chung Cheng University, Taiwan. His research interests include Stability Lobe Diagram database establishment and calculation of cutting forces in supporting smart machining.  
Email: vitrungkien@gmail.com

**Yung-Chou Kao** is the Professor and Head of the Division of Industry-University Cooperation at the Advanced Institute of Manufacturing with High-tech Innovations (AIM-HI) and a Joint Professor at the Department of Mechanical Engineering, National Chung Cheng University (CCU), Taiwan. He has also set up the Machinery Value Engineering laboratory at CCU. Prof. Kao had been invited to be the adviser of research organizations in Taiwan, including the Metals Industry Research and Development Centre, and Precision Machinery Research and Development Center. His research interests include VMR-based machine tool simulators, smart digital manufacturing, cutting force-based NC optimization, and computer-aided manufacturing.  
Email: imeyckao@ccu.edu.tw

**Sheng-Jhe Chen** was a former Ph.D. student in the Advanced Institute of Manufacturing with High-tech Innovations (AIM-HI), CCU, Taiwan.  
[sentry46@gmail.com](mailto:sentry46@gmail.com)

**Guo-Hua Feng** is a Professor at the Department of Power Mechanical Engineering, National Tsing Hua University, Taiwan. His research interests include Piezoelectric thin film, Electroactive polymer, Micromachining, Sensors, Microactuators, Ultrasonic devices, and Intelligent machines.  
Email: ghfeng@pme.nthu.edu.tw

**Sung-Yan Tsai** was a former research student in the Department of Mechanical Engineering, CCU, Taiwan.  
Email: qaz75090134@gmail.com

systems under different cutting-force models. The SLDs were obtained under the same radial depth of cut, but their shapes were greatly different because of the adoption of different feeds per tooth. It implies that feed per tooth has a great influence on stability lobes in the occurrence of cutter runout, which well agrees with the conclusion in [7]. Kao et al [12] used a combination method between theory and experiment in the determination of CFCs in ball-end mill processes. The differences in the amplitudes of cutting force are about 14.5% in the feed direction, 23% in the normal direction, and about 30% in the axial direction. Researchers have developed the chatter stability prediction methods for creating the SLDs in milling machines, such as the average tooth angle approach method [5,6], the frequency domain method [7,8,13,14], semi-discretization method (SDM) [15-16], and full-discretization method (FDM) [17-18-22-41], etc. There have also been several studies of SLD on the turn-mill machine. For example, Kara and Budak [19] studied the optimization of turn-milling processes. The Tool life and MRR (material removal rate) could be increased by 30% and 4%, and the surface roughness, circularity error, and resultant cutting force could be decreased by 130%, 17%, and 5% for this circumstance respectively. Sun et al [18] used the complete discretization method and showed that the SLD for orthogonal turn-milling could reflect the practical machining chatter phenomena. Yan et al [20] studied the effect of variable cutting depth and thickness on milling stability for orthogonal turn-milling. When the diameter ratio of the workpiece and the tool is smaller than 5, the difference in stability boundary is more than 10%. When the diameter ratio of the workpiece and the tool is greater than 5, the difference in stability boundary is less than 10%. Zhan et al. [21] observed that the milling system is greatly improved by using the variable pitch tool and combinations with a wide range of lead angle and tilt angles can be selected to avoid milling chatter. Tang et al [22] studied five-axis milling at low spindle speed, in which the process damping cannot be ignored by instability analysis. They used the full discretization method to solve the SLD. Wang, Gao, and Zheng [23] concluded that altering the milling parameters does not change the milling force coefficients when the selected tool stably cut a workpiece made of the given material. Özşahin and Budak [24] showed the spectrum of sound harmonics that spread on either side of the chatter frequency at tooth passing frequency intervals. The measured cutting force for the chatter-free cutting conditions was at 17142 rev/min with a 5.75mm radial depth of cut.

To sum up, most of the past methods used for the development of SLD were based on both cutting tests and tapping tests on the same machine tool [1-45]. Kao et al

[46] established the relationship between the cutting forces and the surface roughness, their methods use cutting tests and tapping-tests conducted on different CNC machines tools. The prediction accuracy of the surface roughness Ra was above 85% and the maximum error was below 0.893mm. And in the unstable zone, it could also have good accuracy than the stability lobe diagram. It seems that there are seldom papers discussing the influence of CFCs on inter-machine tools and also the related SLDs. Table 1 summarizes some of these papers.

**Table 1.** Number of CNC machines used in the experiment of previous studies

Tool type	Workpiece	Machine	Cutting Type	Reference	Mach	Year
Ball/Flatend	Titanium (TiAl <sub>6</sub> V)	VMC3	S, Up, Down	1,3,4,8	1	1995-1998
Helix end mill	-	VMC5	-	9	1	2007
Flatend, plunge mill	Al 7075	VMC3	S, Up, Down Plunge Milling	2,11,24, 26,27	1	1996-2018
Flatend, Rigid end mill, Ballend	Al7075	VMC5	S, Up, Down	21,25,28,29	1	2018-2020
Ballend	Grey cast Iron FC25	VMC3	S	12	1	2015
Helix end mill	Al6061	VMC,VMC5	Up, Down	13,30	1	2013-2018
Ballend	A5052	VMC	Various tool inclination angles	10	1	2009
Turning Tool insert	AlSi 1050	TMM	-	19	1	2015
Turning Tool insert	Titanium alloy TC21	TMM	-	18	1	2019
Turning Tool insert	Steel 300M	TMM	-	20	1	2016
Bullnose end	AerMet100 steel material	Five-axis CNC machines	-	22	1	2021
Flatend	Aluminum	VMC	Up, Down	31,14,32	1	2006-2010
Turning Tool insert	AlSi 1045	TMM	-	33,34	1	2010
Turning Tool insert	AlSi 1050	Parallel Turning	-	35,36,37	1	2011-2017
Flatend	Aluminium 5083	VMC	-	38	1	2008
End Mill cutter	Hardened mild steel	VMC	Slotting	39	1	2020
General End Mill	AL7075-T6	High-speed multi-axis	Variable helix angle	40	1	2016
Ballend	AlSi 1045	VMC5	-	41	1	2018
Turning Tool insert	S45C	High-speed lathe	-	42	1	2019
Flatend, Turning insert	Al 7075	VMC5	Face mill,	43,44	1	2020
Turning Tool insert	CuZn35	Turning center	-	45	1	2020
Flatend	Copper	VMC & TMM	Down	46	2	2020

VMC: Vertical Milling Center, VMC3: Three-axis VMC, VMC5: Five-axis VMC

S: Slotting, Up: Up milling, Down: Down milling, "-": Not available cutting type

Mach: Number of the CNC machines used for the experiment, TMM: Turn-Milling Machine

In the case of a small-workspace multi-axis MTM, if the workspace is not spacious enough to accommodate a dynamometer, the development of stable machining based on SLDs through cutting test and tapping test is unfeasible. Therefore, the development of SLD alike for stable machining on a multi-axis MTM with small space has been the motivation of this paper. A method is proposed wherein the CFCs are obtained from the cutting tests conducted on the other vertical milling machine centers (VMCs) that have a dynamometer installed for the development of SLD alike towards stable cutting on the MTM in combination with the results of the tapping test

conducted on the MTM.

In this paper, a seven-axis mill-turn machine tool “TA20 MTM” is used as a case study. To create SLD alike for the TA20 MTM, some parameters such as tooth-passing frequency response function (FRF), tool geometry, cutting conditions, and CFCs are required. The tapping test is conducted to obtain the FRF of the TA20 MTM, and the CFC’s were obtained based on the cutting test on the other VMCs. The organization of this paper is as follows. Section 2 introduces the basic theory of stable machining, Section 3 describes the experiment and Section 4 is the result and discussion. Section 5 is the conclusion.

### Introduction of Stable Machining

Flat end mills have been popularly used for general milling applications including slotting, half-up, and half-down milling. It can have variable helix end mills that reduce chatter and vibration on the cutting. Coatings can be applied over it for higher feed rate, speed, and tool life, for fast cuts with the greatest rigidity. In this paper, the flat end mill was selected for studying stable machining.

### Identification of Cutting Force Coefficients in Helical Flat End Mill

Traditionally, the procedure for determining the CFCs is shown in Figure 1. Firstly, the stable cutting parameters were determined by following the tool maker’s recommendations and/or practical experiences for paired tool and workpiece materials, and then cutting tests were conducted. This work selected the depths of cut and spindle speeds to avoid the chatter and reduce the vibrations. Next, the cutting tests at a different feed per tooth  $f_t$  were conducted, and then the CFCs were generally calculated from the experimental data [47] via linear regression.

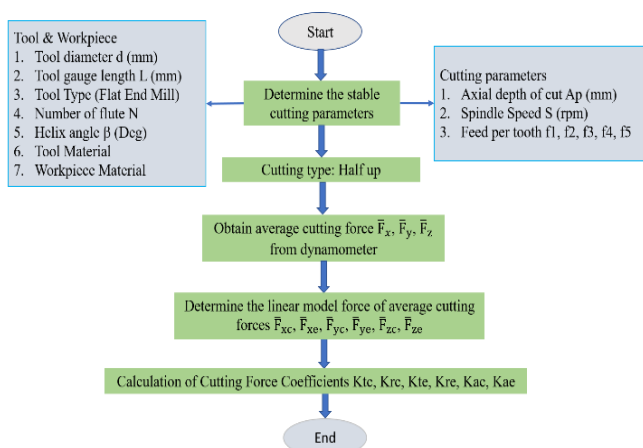


**Figure 1.** Flow chart for determination of Cutting Force Coefficients (CFCs)

The cutting forces with start angles ( $\phi_{st}$ ) and exit angles ( $\phi_{ex}$ ) [47] can be expressed by Equations (1) ~ (3).

$$\bar{F}_x = \left\{ \frac{SAP f_t}{8\pi} [K_{tc} \cos 2\phi - K_{rc} (2\phi - \sin 2\phi)] + \frac{SAP}{2\pi} [-K_{te} \sin \phi + K_{re} \cos \phi] \right\}_{\phi_{st}}^{\phi_{ex}} \quad (1)$$

$$\bar{F}_y = \left\{ \frac{SAP f_t}{8\pi} [K_{tc} (2\phi - \sin 2\phi) + K_{rc} \cos 2\phi] - \frac{SAP}{2\pi} [K_{te} \cos \phi + K_{re} \sin \phi] \right\}_{\phi_{st}}^{\phi_{ex}} \quad (2)$$

$$\bar{F}_z = \frac{SAP}{2\pi} (-f_t K_{ac} \cos \phi + K_{ae} \phi)_{\phi_{st}}^{\phi_{ex}} \quad (3)$$

The average cutting forces can also be expressed by a linear function of feed per tooth  $f_t$  and an offset contributed by the edge forces are as follows [47]:

$$\bar{F}_x = \bar{F}_{xc} f_t + \bar{F}_{xe} \quad (4)$$

$$\bar{F}_y = \bar{F}_{yc} f_t + \bar{F}_{ye} \quad (5)$$

$$\bar{F}_z = \bar{F}_{zc} f_t + \bar{F}_{ze} \quad (6)$$

The average force at each feed per tooth can be measured by a dynamometer in the experiment cutting test, and the components  $\bar{F}_{qc}$ ,  $\bar{F}_{qe}$  ( $q = x, y, z$ ) from Equation (4) to Equation (6) is estimated by linear regression. Finally, the CFCs ( $K_{rc}, K_{tc}, K_{ac}, K_{re}, K_{te}, K_{ae}$ ) are calculated by the combined analysis of experiments and theory, as shown from Equation (7) to (12) in Table 2, using half-up milling as an example where the entry and exit angles are  $\phi_{st} = 0$  and  $\phi_{ex} = \pi/2$  respectively. For half-down milling, the entry and exit angles are  $\phi_{st} = \pi/2$  and  $\phi_{ex} = \pi$  respectively; and for slotting milling the entry and exit angles are  $\phi_{st} = 0$  and  $\phi_{ex} = \pi$  respectively.

**Table 2.** Calculation of cutting force coefficients (CFCs) in Half-up milling

CFCs	Half-up milling	Eqn
$K_{rc}$	$-\left(\frac{2\bar{F}_{yc}}{\pi} + \bar{F}_{xc}\right) / \left(\frac{N_t A_p}{8} + \frac{N_t A_p}{2\pi^2}\right)$	(7)
$K_{tc}$	$-\frac{4\pi}{N_t A_p} \left(\bar{F}_{xc} + \frac{N_t A_p}{8} K_{rc}\right)$	(8)
$K_{re}$	$\frac{-\pi(\bar{F}_{xe} + \bar{F}_{ye})}{N_t A_p}$	(9)
$K_{te}$	$-\frac{2\pi}{N_t A_p} \left(\bar{F}_{xe} + \frac{N_t A_p}{2\pi} K_{re}\right)$	(10)
$K_{ac}$	$\frac{2\pi \bar{F}_{zc}}{N_t A_p}$	(11)
$K_{ae}$	$\frac{4\bar{F}_{ze}}{N_t A_p}$	(12)

### Dynamic Cutting Force in Helical Flat End Mill

This study predicted the dynamic cutting force in the milling process by using a flat end mill tool with a helix angle and the workpiece material is copper. The helical flat end mill geometry is illustrated in Figure 2. The axial depth is sectioned into multiple slices with thickness  $dz$ . The delay distance  $r\chi = r d\phi$  which becomes the angular delay between slices. The value of  $\chi$  can be calculated by Equation (13).

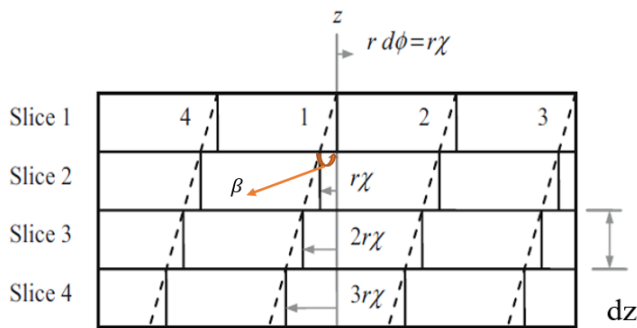


Figure 2. Helical flat end mill geometry [48]

$$\chi = \frac{dz \cdot \tan(\beta)}{r} = \frac{2dz \cdot \tan(\beta)}{d} \text{ (rad)} \tag{13}$$

By substituting  $d\phi$  for  $\chi$ , the  $dz$  could be calculated,

$$dz = \frac{d \cdot d\phi}{2 \tan(\beta)} \tag{14}$$

The cutting forces in milling could be calculated by Equation (15) [48]. In Equation (15) and Equation (16) when the chip thickness  $h(t)$  is the static chip thickness, the cutting forces are the static cutting forces; and when the chip thickness  $h(t)$  is the dynamic chip thickness, the cutting forces become the dynamic cutting forces. In Equation (17), the vibrations in the direction of the surface normal for the current tooth depend on the  $x$  and  $y$  vibrations as well as the tool angle.

$$\begin{Bmatrix} F_x \\ F_y \\ F_z \end{Bmatrix} = \begin{bmatrix} \cos(\phi_a) & \sin(\phi_a) & 0 \\ \sin(\phi_a) & -\cos(\phi_a) & 0 \\ 0 & 0 & -1 \end{bmatrix} \begin{Bmatrix} F_t \\ F_n \\ F_a \end{Bmatrix} \tag{15}$$

where 
$$\begin{cases} F_t = K_{tc}h(t)A_p + K_{te}A_p \\ F_n = K_{rc}h(t)A_p + K_{re}A_p \\ F_a = K_{ac}h(t)A_p + K_{ae}A_p \end{cases} \tag{16}$$

$$\begin{cases} h(t) = f_t \sin(\phi_t) + n(t - \tau) - n(t) \\ \tau = \frac{60}{SN_t} \\ n(t) = x \sin(\phi_t) - y \cos(\phi_t) \end{cases} \tag{17}$$

### Experiment

Since the dynamometer is not feasible to be installed in the available workspace for the adopted seven-axis mill-turn machine tool TA20 MTM, so the experiments were conducted in the following sequences in this study. Firstly, the tapping test experiment was conducted on the TA20 MTM to get the FRF. Cutting tests were performed on the other vertical milling machines (VMCs) for the identification of CFCs. Then, machining was conducted on TA20 MTM and the surface roughness was measured for indirect observation of stable and unstable cutting towards the applicable inter-machine tool stable machining.

### Experimental Design

Since the cutting tests cannot be conducted on the adopted machine tool TA20 MTM, the CFCs obtained in this study are based on the cutting tests conducted on the other VMC machines. The identification of CFCs was then calculated and used for the TA20 MTM. The experiments were conducted in the following sequence as shown in Figure 3. At first, experiments were conducted to choose different cutting parameters at one of the VMC machines, and then the cutting forces were measured by a tri-axial dynamometer; after that, the same method described in Section 2.1 was used to calculate the CFCs in  $X$ ,  $Y$ , and  $Z$  direction. The same experiments were repeated for the other two VMCs. Secondly, a tapping test was conducted at the tool point in the  $X$  and  $Y$  direction at the TA20 MTM to get the tool point transfer function followed by the identification of the dynamic parameter of FRF in the  $X$  and  $Y$  direction. Finally, The CFCs obtained from the cutting test on the other VMCs and FRF on TA20 MTM were adopted to create the SLDs for TA20 MTM. The derivation of the stability lobe diagram is described in Appendix A for reference.

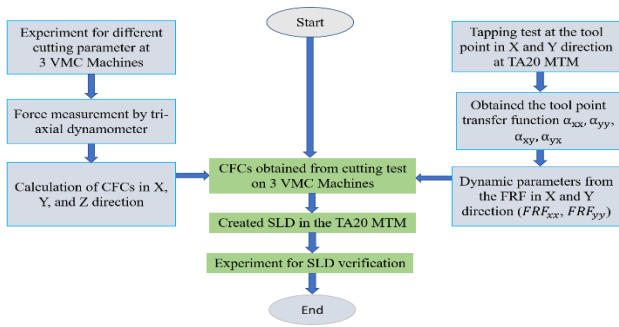


**Figure 3.** Flow chart of the experiment for SLD

*Tapping Test*

This research used an integrated measurement system that consisted of the acceleration sensor (ENDEVCO-25B-10668), hammer (KISTLER-9722A2000), and DAQ (NI 9234). And Cutpro™ software was used to analyze the FRF. The detailed settings of the measurement experiment are illustrated on the left-hand side of Figure 4. The tool is struck using a hammer to exert impacts on the tool; then an accelerometer attached to the tool is used to obtain the tool vibration signals, and the data is collected through a data acquisition (DAQ) device. Finally, using the tapping test module (MALTF) in Cutpro™ software, the FRF results could be generated, as are displayed on the right-hand side of Figure 4, Table 3, and Table 4.

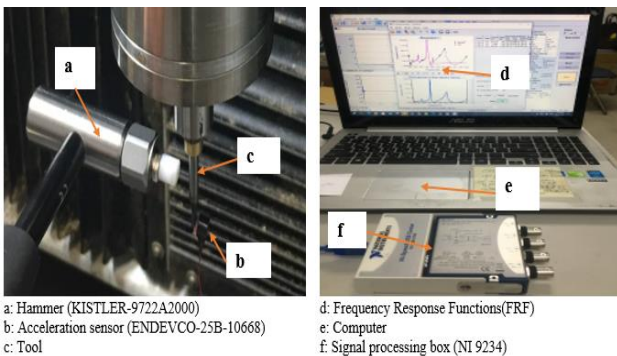


**Figure 4.** Tapping test at TA20 MTM

**Table 3.** The parameter of FRF processing in the Y direction

	Direction XX	Direction YY
Frequency (Hz)	3025.2629	3130.5699
Damping Ratio (%)	3.413	4.736
Modal Stiffness (N/m)	4.1961E+06	4.4483E+06
Mass (Kg)	0.0116	0.0115

**Table 4.** The parameter of FRF processing in X the direction

	Direction XX	Direction YY
Frequency (Hz)	3130.5699	3025.2629
Damping Ratio (%)	4.736	3.413
Modal Stiffness (N/m)	4.4483E+06	4.1961E+06
Mass (Kg)	0.0115	0.0116

*Cutting test at the other Vertical Milling Machine Center (VMC)*

The dynamometer used in the cutting test is type XYZ FORCE SENSOR, model 624-120-5KN. The cutting experiment is used mainly to obtain six CFCs - Kae, Kac, Kre, Krc, Ktc, and Kte on the VMCs. This research establishes the SLD for copper material on the TA20 MTM. The cutting experiment is half up milling, the tool type is flat end mill. The cutting conditions are shown in Table 5, and the tool is Tungsten Carbide. The specifications for the other three VMCs are shown in Table 6. Both VC608 and NDV102A are general vertical machine center while DTC500 is a tapping center.

**Table 5.** Cutting conditions for half up milling

Cutting Test	1	2	3	4.	5
Tool diameter [mm]	3	3	3	3	3
Number of flutes	2	2	2	2	2
Helix angle [deg]	35	35	35	35	35
Axial depth of cut [mm]	0.5	0.5	0.5	0.5	0.5
Feed per tooth [mm/tooth]	0.012	0.014	0.016	0.018	0.020
Spindle speed [rpm]	5120	5120	5120	5120	5120

**Table 6.** The specifications of the other VMC machines

Specifications	X/Y/Z-axis travel	X/Y/Z-axis rapid	Max spindle speed
Machine			
VC608 [49] Machining Center	850/610/530 (mm)	24/24/24 (m/min)	12000 (rpm).
NDV102A [50] Machining Center	1020/600/600 (mm)	24/24/24 (m/min)	12000 (rpm).
DTC500 [51] Tapping Center	610/350/380 (mm)	24/24/24 (m/min)	10000 (rpm)

### The Workspace Issue

This research adopted a TA20 MTM manufactured by Arix Machinery Co. Ltd. for the case study. The specifications of this machine are: X/Y/Z-axis travel (mm): 100/200/200 mm; X/Y/Z-axis fast speed: 10/10/10 m/min; maximum spindle speed: 30000 rpm. The limited workspace of the TA20 MTM is 400/300/100 (mm) and is shown by the blue block in Figure 5.

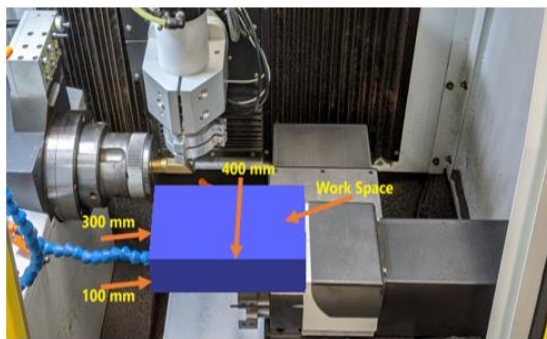


Figure 5. The workspace of the adopted TA20 MTM

The dynamometer models used in this research are Kistler 9265B and 9443B; the size of it is 220 mm \* 100 mm \* 186 mm, as shown in Figure 6. It can be seen from Figure 5 and Figure 6 that the Kistler dynamometer (9265B and 9443B) is too large to be installed in the workspace of TA20 MTM. This will lead to the problem that the cutting force signal cannot be obtained by cutting test directly on TA20 MTM.

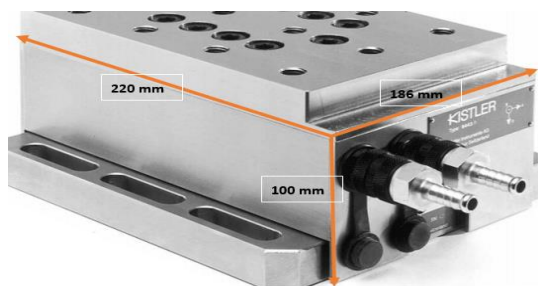


Figure 6. Kistler dynamometer models: 9265B and 9443B

### Cutting Experiment for Applicability of Inter-machine Tool SLDs

More cutting experiments were planned to study the applicability of SLD for a machine tool with its FRF and CFCs from the other machine tools. The cutting experimental parameters for the TA20 MTM include eight spindle speeds and eight cutting depths; and therefore, sixty-four cutting conditions, as listed in Table 7. The machined surface roughness [52] was measured to study the inter-machine tool applicability.

Table 7. The cutting conditions of the designed experiments

Spindle speed S (rpm)	Depth of cut $A_p$ (mm)
5000	0.1
7000	0.3
9000	0.5
11000	0.7
13000	0.9
15000	1.1
17000	1.3
19000	1.5

In these experiments, the cutting width ( $A_e$ ) was designed to be equal to the cutting depth ( $A_p$ ). The workpiece was a copper rod, with a diameter of 20 mm and a length 100 mm. Before conducting the cutting, the copper rod was milled into an inclined plane to ease the setting of  $A_p = A_e$  and subsequent surface roughness measurement. These machining experiments were carried out by milling in the Y direction, and eight layers were cut. The eight layers of cut corresponding to different depths of cuts are shown in Figure 7.

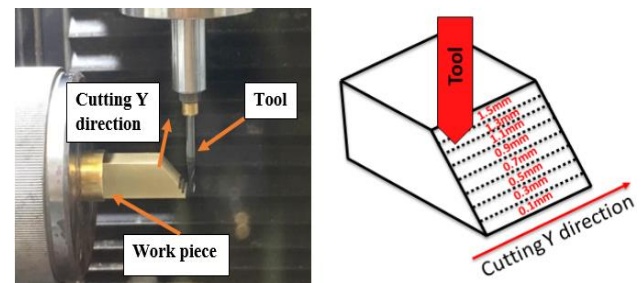


Figure 7. Cutting experiments with  $A_p = A_e$

### Result and Discussion

Three VMCs as listed in Table 6 were adopted for the cutting test to obtain three sets of the CFCs to study the applicability of stable machining in this research on TA20 MTM with limited workspace. To save space in this paper, only the CFCs obtained from the cutting test in VC608 are adopted for the explanation. Sections 4.1 and Section 4.2 discuss the correctness and verification of the results. Section 4.3 describes the inter-machine tool applicability of stable machining based on SLD for TA20 MTM by surface roughness  $R_a$  measured from a series of cutting experiments, as is described in Section 3.5. The SLD were generated by the FRF (measured in TA20 MTM) and three sets of CFCs from the adopted other VMCs respectively.

### The results of CFCs and Cutting Force

The calculation of CFCs is based on the measured cutting forces obtained from the dynamometer during the cutting tests and then analyzed by linear regression. The cutting parameters shown in Table 5 were used in this study. After analyzing the cutting forces resulting from cutting tests on the VMCs listed in Table 6, the best line that passes through the values of average cutting forces was selected; and then linear regression was used for determining the components of the linear forces ( $\bar{F}_{xc}$ ,  $\bar{F}_{xe}$ ,  $\bar{F}_{yc}$ ,  $\bar{F}_{ye}$ ,  $\bar{F}_{zc}$ , and  $\bar{F}_{ze}$ ). The formula for calculating CFCs has been described from Equation (7) to (12) in Section 2.1. The calculated results of CFCs based on the cutting tests on the VC608 with the helical flat-end mill are compared with the calculated CFC resulting from that using the Cutpro™ software; and the comparison is found to be in good agreement with the result Ref [3, 12], as shown in Table 8. The absolute values of CFCs of “VC608” and the “Cutpro™” only had a small difference. For each CFC, the absolute value in “VC608” is larger than that in the “Cutpro™”. The maximum difference is about 0.12%, and the minimum difference is about 0%. That is to say, the accuracy rate of the CFC results in this paper compared with CFC in Cutpro™ software could be reached at about 99.88% for the case of half up milling on VC608.

**Table 8.** Comparing CFCs vs. that from Cutpro™ on VC608

CFCs [N/mm <sup>2</sup> ]	CFCs (VC608)	CFCs (Cutpro™)	Difference (%)
Ktc	1030.13	1030.01	0.12
Krc	618.02	617.96	0.06
Kac	235.04	235.01	0.03
Kte	7.05	7.05	0
Kre	5.38	5.38	0
Kae	0.10	0.1	0

In the result of [12], the differences are about 14.5% in the feed direction, 23% in the normal direction, and about 30% in the axial direction. The comparison of cutting forces on VC608 between this research and that measured from the dynamometer (Real), and the result Ref [3,12] is shown in Figure 8 to check the correctness of estimated (calculated) cutting forces in the directions of “Feed”, “Normal”, and “Axial”, respectively. The cutting forces for three revolutions are shown in Figure 8. The “blue” line is the cutting force in feed direction Fx, the “green” line is the cutting force in normal direction Fy, and the “red” line is the cutting force in axial direction Fz calculated in this research. While the Fx, Fy, and Fz obtained from the dynamometer (Real) is shown in “orange”, “purple”, and “yellow” lines, respectively. The comparison in Figure 8 shows reasonably good agreement

between the calculated values and the measured values from the dynamometer.

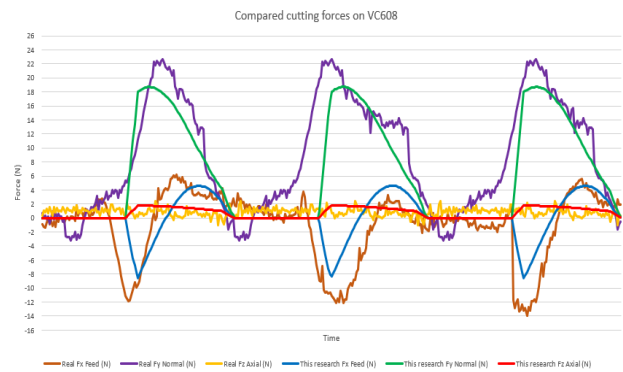


**Figure 8.** Comparing cutting forces between estimated (this research) and the real on VC608

### Stable and Unstable Cutting through Observing Cutting Force

In this study, the CFCs were obtained from a series of half-up milling cutting tests according to the cutting conditions shown in Table 5. The SLD, as shown in Figure 9, for TA20 MTM was generated by using Cutpro™ with the synergy of the FRF of the TA20 MTM obtained from the tapping test and the CFCs of VC608. The estimated cutting forces of Fx for twenty individual revolutions are also shown in Figure 9 for the same depth of cut  $A_p = 0.9$  mm and at three different spindle speeds  $S = 9500, 13000,$  and  $18000$  rpm. It can be seen that when  $A_p = 0.9$  mm, the helical end milling process is unstable (according to SLD) at  $S = 9500$  rpm; it is observed that the feed direction force (Fx) changes rapidly from -50N to 300N. At the same depth of cut  $A_p=0.9$  mm, the cutting is stable (according to SLD) when  $S=13000$  rpm and  $S=18000$ ; it is observed that the cutting force in the feed direction (Fx) does not change rapidly, as the result Ref[4]. This might mean unstable cutting could occur if the cutting force changes very rapidly.

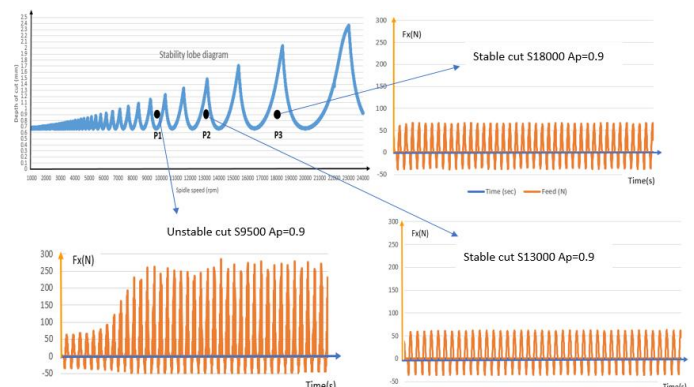


**Figure 9.** Observing stable and unstable cutting on TA20 MTM via changes of cutting forces, Ref [4]



### Applicability of Stable and Unstable Cutting on TA20MTM through SLDs and Ra

The CFCs are important input parameters for developing SLDs. The CFCs according to the cutting tests on the VMCs listed in Table 6 are shown in Table 9. The CFCs on VC608, NDV102A, and DTC500 are quite different from each other. This means that CFCs are affected by the characteristics of the adopted VMC. Furthermore, the SLDs generated by using the three sets of CFCs in Table 9 and the FRF of TA20 MTM in Table 3 are shown in Figure 10a. Although their wavy shapes of them are similar to each other, the SLDs are different from each other. For example, the critical depth of cut ( $b_{lim}$ ) of these SLDs in Figure 10a is about 0.65mm (for VC 608), 0.58mm (for NDV102A), and 0.37mm (for DTC500) respectively; The tapping center DTC500 has the lowest critical depth of cut. This might result from the general weaker comprehensive structural rigidity of a tapping center. In addition, the SLDs generated by using the three sets of CFCs in Table 9 and the FRF of TA20 MTM in Table 2 and Table 3 are shown in Figure 10b. This shows that different FRF result in different SLDs and the critical depth of cut is also different. It might mean that the optimum critical depth of cut in machining could be different in the different axial directions.

**Table 9.** The results of CFCs at adopted 3 VMCs for developing SLDs, as the results CFCs from Cutpro™

CFCs \ VMCs	VC608	NDV102A	DTC500
Ktc	1030.01	1198.14	1825.02
Krc	617.96	372.29	940.68
Kac	235.01	519.87	501.77
Kte	7.05	0.03	-5.53
Kre	5.38	11.85	8.86
Kae	0.10	-2.75	-6.73

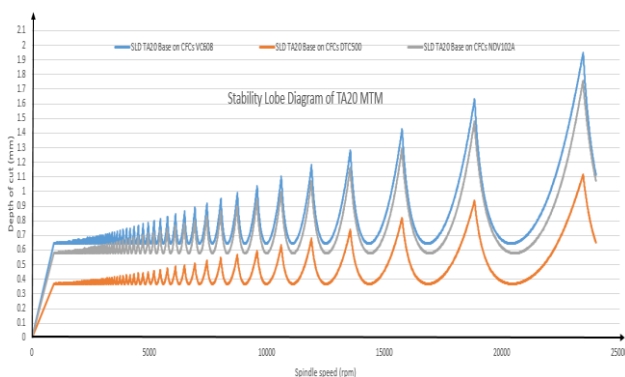


**Figure 10a.** Three SLDs of TA20 MTM – Processing in the Y direction

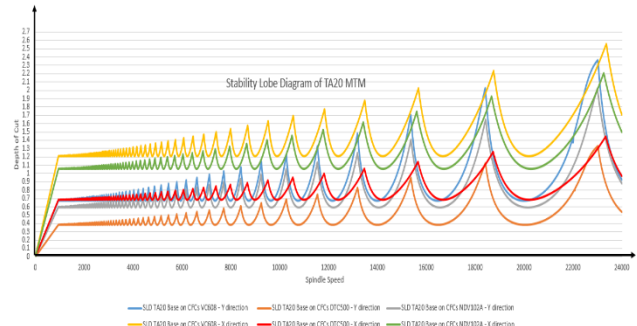


**Figure 10b.** Six SLDs of TA20 MTM – in Y and X direction

From the Modal analytical stability lobes in Cutpro™, the critical depth of cut corresponding to the eight selected spindle speeds (5000, 7000, 9000, 11000, 13000, 15000, 17000, 19000 rpm) were noted; and eight graphs, as shown in Figure 11, are plotted to show the variations of critical depth of cut  $A_p$  (0.1, 0.3, 0.5, 0.7, 0.9, 1.1, 1.3, 1.5 mm) versus radial width of cut  $A_e$  at a particular spindle speed respectively. These data were generated by using Cutpro™. The depth of cut was intentionally assigned to be equal to the width of cut, i.e.  $A_p=A_e$ . For explanation purposes, Figure 12 shows the SLD generated from Cutpro™ based on the CFC of VC608 and FRF of TA20 MTM. It also shows that the critical depth of cut  $A_p$  is 0.9193 mm when the width of cut  $A_e$  is 1.1 mm and spindle speed is 4945 (about 5000) rpm. In Figure 11, the processed experiment used eight different speeds for machining from S=5000 to S=19000 rpm and the cutting width ( $A_e$ ) was selected to be equal to the cutting depth ( $A_p$ ). It shows the variation of critical depth of cut for the adopted three different VMCs corresponding to different spindle speeds (S). The orange line represents the variation of critical depth of cut for the NDV102A, the grey line represents the variation of critical depth of cut for the VC608, and the blue line represents the variation of critical depth of cut for the DTC500, and the yellow line represents the cutting experiment. It is found that these three curves (the orange, grey, and blue curves) seem to overlap each other starting from the middle to the lower right. Furthermore, the area after the intersection of plots of these three curves and that from the cutting experiment (yellow line) forms the unstable cutting region, and the region to the left of the overlapped point represents the stable cutting.

Figure 13 is the 3D form merging the sub-figures in Figure 11. The red surface represents the variation of critical depth of cut for the NDV102A machine, the green surface represents the variation of critical depth of cut for the VC608 machine, the blue surface represents the variation of critical depth of cut for the DTC500 machine, and the yellow surface represents the variation from the cutting experiment.

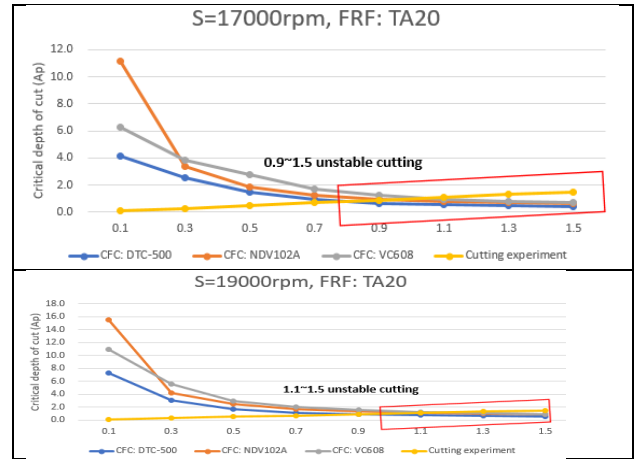
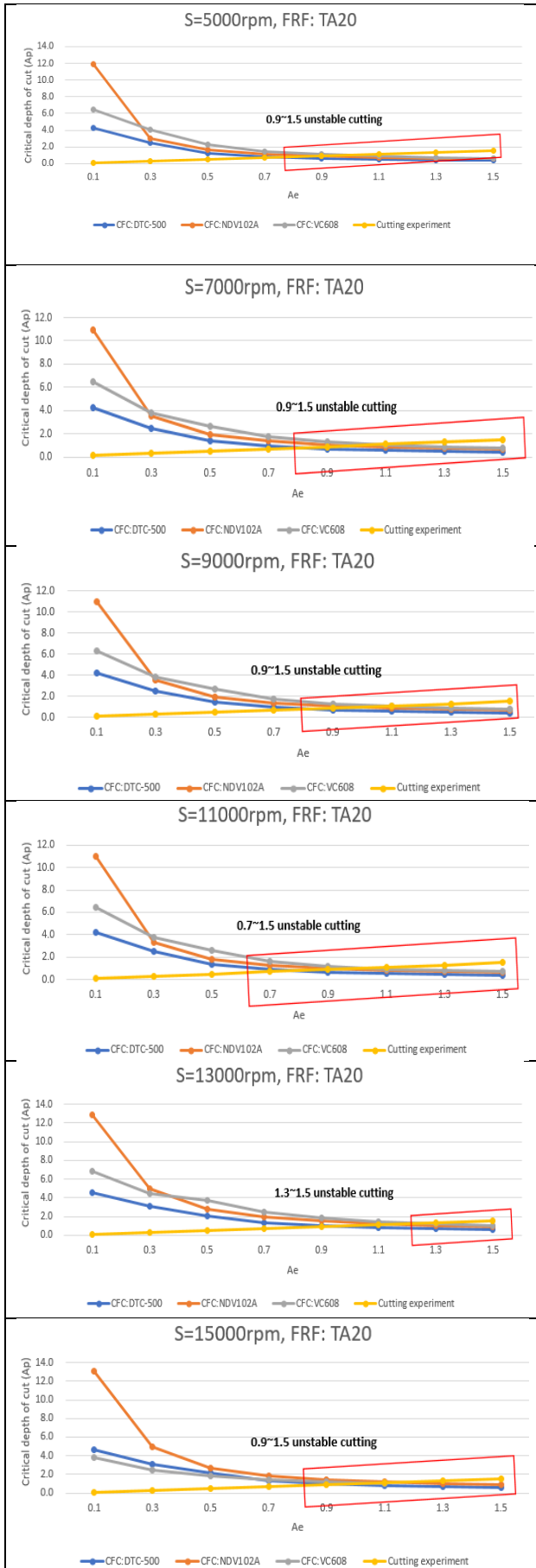


**Figure 11.** Verification of stable and unstable cutting on TA20 MTM

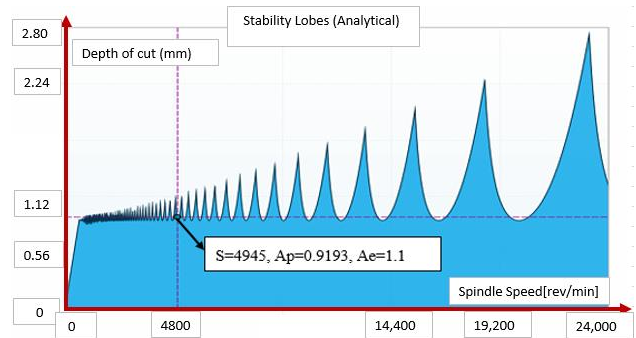


**Figure 12.** Example of the critical depth of cut  $A_p$  corresponding to  $S$  and  $A_e$

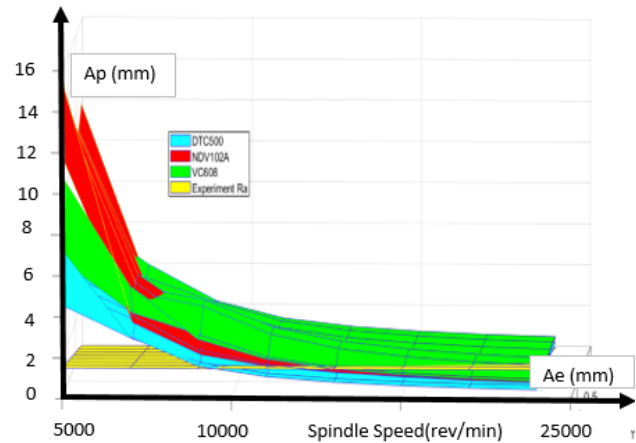


**Figure 13.** A 3D form showing the critical depth of cut using different CFCs and the same FRF

With the consideration of repeatability, each of the above sixty-four conditions was cut three times, and it means altogether 192 experiments were conducted. Surface roughness was used to further study the SLD applicability of TA20 MTM since three different SLDs could be created, as shown in Figure 10. Surface roughness is an important index for industrial production application and

international standards had been published, for example, the ISO 4287:1997[53]. Therefore, measurement of roughness was planned to correlate with the cutting quality. The Ra of the workpiece was measured by using the surface roughness instrument Mitutoyo, model SJ-410 [54], and the result is shown in Table 10.

Interestingly, in tradition, the expected ranges of Ra for the average application of milling machining are from 0.8 to 6.3 μm [55], as shown in Figure 14; therefore, roughness Ra = 0.8 μm was adopted in this study trying to explore characteristics to differentiate stable and unstable milling quality. That is to say, this paper assumes the range belongs to a stable zone if the Ra < 0.8 μm, and the range belongs to an unstable zone if Ra ≥ 0.8 μm. Therefore, according to Table 10, the experimental results are summarized in Table 11 where “O” denotes stable cutting “Ra < 0.8 μm”, and “X” denotes unstable cutting “Ra ≥ 0.8 μm”. The relationship is depicted in Figure 15 to ease the understanding related to the depth of cut and spindle speed. It is obvious that the trend line “ $y=2E-05x + 0.4393$ ” is almost inside the stable zone. This means that stable machining could be achieved when Ra = 0.8 if the average application of milling is used although it seems to be a bit conservative because the critical depth of cut is 0.5 mm. Certain adjustable spaces exist between the lower green trend line “ $y=2E-05x + 0.4393$ ” and the upper red trend line “ $y=2E-05x + 0.6393$ ”. It is also very interesting that the critical depth of cut 0.5 mm is also located in the stable zone of Figure 11.

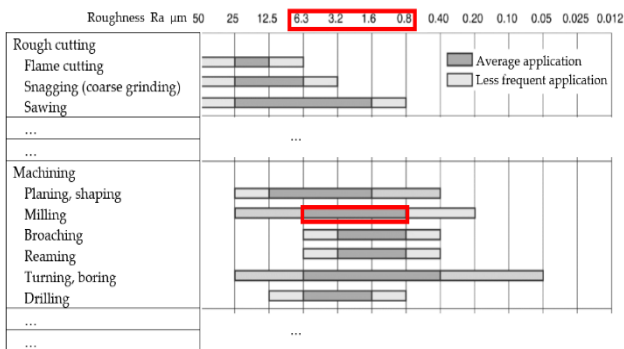


**Figure 14.** The average application roughness (Ra) ranges of milling [55]

**Table 10.** Workpiece surface roughness Ra (μm)

S (rpm)	n <sup>th</sup> cut	A <sub>p</sub> (mm)							
		0.1	0.3	0.5	0.7	0.9	1.1	1.3	1.5
5000	1	0.300	0.733	0.756	0.977	8.802	7.351	2.558	6.175
	2	0.344	0.638	0.776	0.999	8.177	6.628	2.980	4.392
	3	0.318	0.602	0.733	0.947	5.091	8.685	7.384	5.217
7000	1	0.349	0.461	0.525	0.993	1.481	1.242	2.394	3.689
	2	0.445	0.491	0.527	0.954	1.534	1.879	2.894	2.547
	3	0.325	0.689	0.538	0.923	1.242	1.450	4.666	2.409
9000	1	0.244	0.374	0.638	0.972	2.307	2.108	2.091	2.633
	2	0.223	0.377	0.552	0.785	2.145	2.339	3.789	4.024
	3	0.281	0.540	0.661	0.587	2.263	5.895	3.690	2.576
11000	1	0.193	0.449	0.631	0.938	1.198	2.070	0.917	1.254
	2	0.230	0.449	0.662	1.072	1.304	2.836	0.987	1.997
	3	0.272	0.502	0.674	0.954	1.344	2.202	0.916	1.332
13000	1	0.211	0.334	0.559	0.651	0.588	0.743	0.867	2.241
	2	0.214	0.315	0.508	0.642	0.584	0.730	1.039	2.249
	3	0.189	0.353	0.513	0.747	0.562	0.679	1.248	2.071
15000	1	0.216	0.387	0.397	0.637	1.409	0.958	0.712	1.779
	2	0.368	0.347	0.398	0.675	1.324	0.979	1.313	1.959
	3	0.399	0.376	0.420	0.849	1.347	0.989	1.619	1.462
17000	1	0.243	0.480	0.553	1.085	1.081	2.663	1.365	1.966
	2	0.290	0.455	0.577	0.753	1.534	2.259	1.714	1.944
	3	0.303	0.482	0.582	0.956	1.734	2.286	1.741	2.379
19000	1	0.278	0.413	0.392	0.502	0.987	1.458	0.826	1.284
	2	0.290	0.402	0.495	0.650	0.925	1.216	1.065	1.401
	3	0.300	0.388	0.488	0.733	0.813	1.187	1.237	1.103

**Table 11.** The stable and unstable zone at different speeds S and depths of cut A<sub>p</sub>

S (rpm)	A <sub>p</sub> (mm)							
	0.1	0.3	0.5	0.7	0.9	1.1	1.3	1.5
5000	O	O	O	X	X	X	X	X
7000	O	O	O	X	X	X	X	X
9000	O	O	O	X	X	X	X	X
11000	O	O	O	X	X	X	X	X
13000	O	O	O	O	O	O	X	X
15000	O	O	O	O	X	X	X	X
17000	O	O	O	X	X	X	X	X
19000	O	O	O	O	X	X	X	X

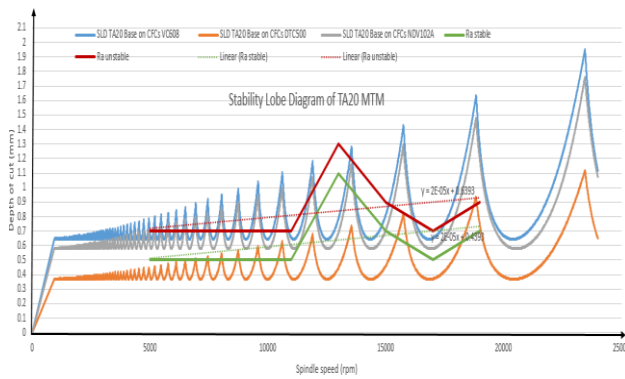


**Figure 15.** The stable and unstable TA20 MTM based on Ra of average application Ref [55]

## Conclusion

It is generally not feasible to install a table-type or rotary dynamometer on a small-workspace MTM such as the adopted small seven-axis mill-turn machine TA20 MTM, the cutting forces could not be measured on such a machine using a dynamometer during the cutting test resulting in the unavailability of obtaining CFCs. However, the generation of SLD needs to have CFCs and FRF; SLD is a comprehensive index very useful for the determination of the most appropriate and effective cutting parameters. This study proposes a new possibility of using CFC's obtained from the cutting tests conducted on the other VMCs that can have a dynamometer installed for CFCs. A case study had been successfully implemented to generate the SLD of TA20 MTM by adopting the cutting force coefficients obtained from the cutting test on the other VMCs (VC608, NDV102A, and DTC500), and FRF developed via tapping test on TA20 MTM. However, the CFCs from the adopted VMCs are different from each other, therefore, surface roughness was adopted to further study the applicability of SLD.

Since the CFCs for the TA20 MTM cannot be directly obtained from the cutting test and therefore SLD for TA20 MTM cannot be generated using conventional methods. However, through the comparative analysis of the SLDs the Ra measured from cutting experiments, the area on the intersection of SLD plots of the other three VMCs was analyzed for the same cutting depths as that of the Ra experiment; unstable and stable cutting regions were successfully identified for TA20 MTM. These have resulted in a new type of SLD for the TA20 MTM, as shown in Figure 16 resulting from Figure 11, Table 11, and Figure 15. This means that the major contribution of this paper is that stable and unstable cutting of a machine tool that could not have a dynamometer installed for the calculation of CFCs based on the cutting test still can have an alternative way if and only if the FRF could be obtained by tapping test on the machine itself. Furthermore, the FRFs based on

the tapping test are different from each other in various axial directions. That is to say, optimum cutting parameters such as the critical depth of cut according to the SLDs, as shown in Figure 10b, are affected by the FRFs since FRFs are different in each axial direction.

Further study will be on extending the proposed methods for the exchangeability of CFCs, FRFs, and so as the SLDs for the machine tool with the same model manufactured by the same machine tool builders.

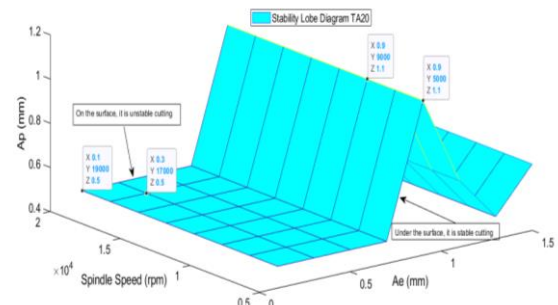


**Figure 16.** Stable and unstable cutting of TA20 MTM

## Appendix

Appendix A (Symbols, The solution of Chatter Stability in Milling).

## Acknowledgments

The authors thank the support from the Ministry of Science and Technology (MOST), Taiwan, under the grant MOST 110-2221-E-194-039- and MOST 110-2634-F-194-005. Appreciation extends to the Advanced Institute of Manufacturing with High-tech Innovations (AIM-HI), National Chung Cheng University (CCU), Taiwan.

## References

- [1] Lee, P and Altintas, Y, "Prediction of ball-end milling force from orthogonal cutting data". *Int. J. Mach. Tools Manufact*, Vol. 36, No. 9, pp. 1059-1072, 1996. [https://doi.org/10.1016/0890-6955\(95\)00081-X](https://doi.org/10.1016/0890-6955(95)00081-X)
- [2] Shirase, K and Altintas, Y, "Cutting Force and dimensional surface error generation in peripheral milling with variable pitch helical end mills", *Int. J. Mach. Tools Manufact*, Vol. 36, No. 5, pp. 567-584, 1996. [https://doi.org/10.1016/0890-6955\(95\)00063-1](https://doi.org/10.1016/0890-6955(95)00063-1)
- [3] Budak, E. Altintas, Y. and E. J. A. Armarego, "Prediction of Milling Force Coefficients from Orthogonal Cutting Data", *Journal of Manufacturing Science and Engineering* 118(2): 216-224, 1996.

<https://doi.org/10.1115/1.2831014>

[4] Altıntaş, Y. and Lee, P, "A General Mechanics and Dynamics Model for Helical End Mills", *CIRP Annals* 45(1): 59-64, 1996.

[https://doi.org/10.1016/S0007-8506\(07\)63017-0](https://doi.org/10.1016/S0007-8506(07)63017-0)

[5] Smith, S., and Tlustý, J, "Update on High-Speed Milling Dynamics". *Journal of Manufacturing Science and Engineering*, 112: 142-149, 1990.

<https://doi.org/10.1115/1.2899557>

[6] Smith, S. and Tlustý, J, "An Overview of Modeling and Simulation of the Milling Process", *Journal of Manufacturing Science and Engineering*, 113: 169-175, 1991. <https://doi.org/10.1115/1.2899674>

[7] Altıntaş, Y., Budak, E, "Analytical Prediction of Stability Lobes in Milling", *CIRP Annals*, Vol. 44, pp. 357-362, 1995.

[https://doi.org/10.1016/S0007-8506\(07\)62342-7](https://doi.org/10.1016/S0007-8506(07)62342-7)

[8] Budak, E. and Altıntaş, Y, "Analytical Prediction of Chatter Stability in Milling-Part II: Application of the General Formulation to Common Milling Systems." *Journal of Dynamic Systems, Measurement, and Control* 120(1): 31-36, 1998.

<https://doi.org/10.1115/1.2801318>

[9] Turner, S., Merdol, D., Altıntaş, Y., and Ridgway K, "Modelling of the stability of variable helix end mills", *International Journal of Machine Tools and Manufacture* 47(9): 1410-1416, 2007.

<https://doi.org/10.1016/j.ijmactools.2006.08.028>

[10] Shamoto, E., and Akazawa, K, "Analytical prediction of chatter stability in ball-end milling with tool inclination", *CIRP Annals* 58(1): 351-354, 2009.

<https://doi.org/10.1016/j.cirp.2009.03.087>

[11] Wan, M., Wang Ting, Y., Hong Zhang, W., and Dang Wei, J, "Prediction of chatter stability for multiple-delay milling system under different cutting force models", *International Journal of Machine Tools and Manufacture* 51(4): 281-295, 2011.

<https://doi.org/10.1016/j.ijmactools.2010.12.007>

[12] Kao, Y- C., Nguyen, Nhu-Tung, Chen, Mau-Sheng, and Huang, Shyh-Chour, "A combination method of the theory and experiment in determination of cutting force coefficients in ball-end mill processes", *Journal of Computational Design and Engineering* 2(4): 233-247, 2015. <https://doi.org/10.1016/j.jcde.2015.06.005>

[13] Sun, Y., and Jiang S., "Predictive modeling of chatter stability considering force-induced deformation effect in milling thin-walled parts", *International Journal of Machine Tools and Manufacture* 135: 38-52, 2018.

<https://doi.org/10.1016/j.ijmactools.2018.08.003>

[14] Altıntaş, Y., Stepan, G., Merdol, D., Dombóvari, Z, "Chatter stability of milling in frequency and discrete time domain", *CIRP Journal of Manufacturing Science and Technology* 1(1): 35-44, 2008.

<https://doi.org/10.1016/j.cirpj.2008.06.003>

[15] Insperger, T. and Stépán, G, "Semi-discretization method for delayed systems", *International Journal for Numerical Methods in Engineering* 55(5): 503-518, 2002.

<https://doi.org/10.1002/nme.505>

[16] Insperger, T. and Stépán, G, "Updated semi-discretization method for periodic delay-differential equations with discrete delay", *International Journal for Numerical Methods in Engineering* 61(1): 117-141, 2004.

<https://doi.org/10.1002/nme.1061>

[17] Ding, Y., Zhu Min, L., Jian Zhang, X., and Ding, H, "A full-discretization method for prediction of milling stability", *International Journal of Machine Tools and Manufacture* 50(5): 502-509, 2010.

<https://doi.org/10.1016/j.ijmactools.2010.01.003>

[18] Sun, T., Fang Qin, L., Can Fu, Y., and Ming Hou, J, "Chatter stability of orthogonal turn-milling analyzed by complete discretization method", *Precision Engineering* 56: 87-95, 2019.

<https://doi.org/10.1016/j.precisioneng.2018.10.012>

[19] Kara, M. E., and Budak, E, "Optimization of Turn-milling Processes", *Procedia CIRP* 33(2015): 476-483, 2015. <https://doi.org/10.1016/j.procir.2015.06.057>

[20] Yan, R., Tang, X.W., Peng, F.Y., Wang, Y and Qiu, F, "The effect of variable cutting depth and thickness on milling stability for orthogonal turn-milling", *The International Journal of Advanced Manufacturing Technology* 82(1-4): 765-777, 2016.

<https://doi.org/10.1007/s00170-015-7418-2>

[21] Zhan, D., Jiang, S., Niu, J., and Sun, Y, "Dynamics modeling and stability analysis of five-axis ball-end milling system with variable pitch tools", *International Journal of Mechanical Sciences* 182: 105774, 2020.

<https://doi.org/10.1016/j.ijmecsci.2020.105774>

- [22] Tang, X., Peng, F., Yan, R., Zhu, Z., Li, Z and Xin, S, "Nonlinear process damping identification using finite amplitude stability and the influence analysis on five-axis milling stability", *International Journal of Mechanical Sciences* 190: 106008, 2021.  
<https://doi.org/10.1016/j.ijmecsci.2020.106008>
- [23] Wang, Minghai, Gao, Lei, Zheng, Yaohui, "An examination of the fundamental mechanics of cutting force coefficients", *International Journal of Machine Tools & Manufacture* 78 (2014) 1-7.  
<https://doi.org/10.1016/j.ijmachtools.2013.10.008>
- [24] Altintas, Y. and J. H. Ko, "Chatter Stability of Plunge Milling", *CIRP Annals*, Volume 55, Issue 1, 2006, Pages 361-364, 2006.  
[https://doi.org/10.1016/S0007-8506\(07\)60435-1](https://doi.org/10.1016/S0007-8506(07)60435-1)
- [25] Özşahin, O., Budak, E., Özgüven, H.N, "Identification of bearing dynamics under operational conditions for chatter stability prediction in high speed machining operations", *Precision Engineering*, Volume 42, October 2015, Pages 53-65, 2015.  
<https://doi.org/10.1016/j.precisioneng.2015.03.010>
- [26] Comak, A., and E. Budak, "Modeling dynamics and stability of variable pitch and helix milling tools for development of a design method to maximize chatter stability", *Precision Engineering* 47: 459-468, 2017.  
<https://doi.org/10.1016/j.precisioneng.2016.09.021>
- [27] Mohammadi, Y., Milad, A., Budak, E, "Suppressing vibration modes of spindle-holder-tool assembly through FRF modification for enhanced chatter stability", *CIRP Annals* 67(1): 397-400, 2018.  
<https://doi.org/10.1016/j.cirp.2018.03.003>
- [28] Tunc, L. T., Mohammadi, Y., Budak, E, "Destabilizing effect of low frequency modes on process damped stability of multi-mode milling systems", *Mechanical Systems and Signal Processing* 111: 423-441, 2018.  
<https://doi.org/10.1016/j.ymsp.2018.03.051>
- [29] Postel, M., Aslan, D., Wegener, K., Altintas, Y, "Monitoring of vibrations and cutting forces with spindle mounted vibration sensors", *CIRP Annals* 68(1): 413-416, 2019. <https://doi.org/10.1016/j.cirp.2019.03.019>
- [30] Budak, E., Comak, A., Ozturk, E, "Stability and high performance machining conditions in simultaneous milling", *CIRP Annals* 62(1): 403-406, 2013.  
<https://doi.org/10.1016/j.cirp.2013.03.141>
- [31] Budak, E, "Analytical models for high performance milling. Part II: Process dynamics and stability", *International Journal of Machine Tools and Manufacture*, Volume 46, Issues 12-13, October 2006, Pages 1489-1499, 2006. <https://doi.org/10.1016/j.ijmachtools.2005.09.010>
- [32] Özşahin, O., Özgüven, H.N., and Budak, E, "Analysis and compensation of mass loading effect of accelerometers on tool point FRF measurements for chatter stability predictions", *International Journal of Machine Tools and Manufacture* 50(6): 585-589, 2010.  
<https://doi.org/10.1016/j.ijmachtools.2010.02.002>
- [33] Kurata, Y., Doruk Merdol, S., Altintas, Y., Suzuki, N., Shamoto, E, "Chatter Stability in Turning and Milling with in Process Identified Process Damping", *Journal of Advanced Mechanical Design, Systems, and Manufacturing* 4(6): 1107-1118, 2010.  
<https://doi.org/10.1299/jamdsm.4.1107>
- [34] Yang, Y., Muñoz, J., Altintas, Y, "Optimization of multiple tuned mass dampers to suppress machine tool chatter", *International Journal of Machine Tools and Manufacture* 50(9): 834-842, 2010.  
<https://doi.org/10.1016/j.ijmachtools.2010.04.011>
- [35] Budak, E. and E. Ozturk, "Dynamics and stability of parallel turning operations". *CIRP Annals*, Volume 60, Issue 1, 2011, Pages 383-386, 2011.  
<https://doi.org/10.1016/j.cirp.2011.03.028>
- [36] Ozturk, E., Comak, A., Budak, E, "Tuning of tool dynamics for increased stability of parallel (simultaneous) turning processes", *Journal of Sound and Vibration* 360: 17-30, 2016. <https://doi.org/10.1016/j.jsv.2015.09.009>
- [37] Azvar, M., and E. Budak, "Multi-dimensional chatter stability for enhanced productivity in different parallel turning strategies", *International Journal of Machine Tools and Manufacture* 123: 116-128, 2017.  
<https://doi.org/10.1016/j.ijmachtools.2017.08.005>
- [38] Quintana, G., Ciurana, J, "A new experimental methodology for identification of stability lobes diagram in milling operations", *International Journal of Machine Tools and Manufacture* 48(15): 1637-1645, 2008.  
<https://doi.org/10.1016/j.ijmachtools.2008.07.006>
- [39] Paliwal, V., Babu, N.R, "Prediction of Stability Lobe Diagram in High-Speed Milling by Operational Modal Analysis", 48th SME North American Manufacturing Research Conference, NAMRC 48 (Cancelled due to COVID-19), 2020.

<https://doi.org/10.1016/j.promfg.2020.05.049>

[40] Ozkirimli, O., Tunc, L. T., Budak, E, "Generalized model for dynamics and stability of multi-axis milling with complex tool geometries", Journal of Materials Processing Technology 238: 446-458, 2016.

<https://doi.org/10.1016/j.jmatprotec.2016.07.020>

[41] Dai, Y., Li, H., Wei, Z.C., Zhang, H, "Chatter stability prediction for five-axis ball end milling with precise integration method", Journal of Manufacturing Processes 32: 20-31, 2018.

<https://doi.org/10.1016/j.jmapro.2018.01.008>

[42] Hayasaka, T., Jung, H., Azuma, K., Shamoto, E, "Consolidated chatter stability prediction model considering material removing and ploughing processes", Precision Engineering 59: 120-133, 2019.

<https://doi.org/10.1016/j.precisioneng.2019.06.006>

[43] Itoh, M., Hayasaka, T., Shamoto, E, "High-efficiency smooth-surface high-chatter-stability machining of thin plates with novel face-milling cutter geometry", Precision Engineering 64: 165-176, 2020.

<https://doi.org/10.1016/j.precisioneng.2020.03.024>

[44] Itoh, M., Hayasaka, T., Shamoto, E, "Novel geometrical design of turning inserts for high-efficiency smooth-surface high-chatter-stability cutting", Precision Engineering 64: 138-146, 2020.

<https://doi.org/10.1016/j.precisioneng.2020.03.018>

[45] Nam, S., Hayasaka, T., Jung, H., Shamoto, E, "Proposal of novel chatter stability indices of spindle speed variation based on its chatter growth characteristics", Precision Engineering 62: 121-133, 2020.

<https://doi.org/10.1016/j.precisioneng.2019.11.018>

[46] Kao, Y.-C., Chen, S.J., Vi, T.K., Feng, G.H and Tsai, S.Y, "Study of milling machining roughness prediction based on cutting force", in IOP Conference Series: Materials Science and Engineering, Volume 1009, The 5th International Conference on Computing and Solutions in Manufacturing Engineering (CoSME'20), Brasov, Romania, 7-10 October 2020.

<https://doi.org/10.1088/1757-899X/1009/1/012027>

[47] Altintas, Y, Manufacturing Automation: Metal Cutting Mechanics, Machine Tool Vibrations, and CNC Design, 2nd ed., New York: Cambridge University Press; ISBN978-1-00148-0, Chapter 2, Page 47, 2012.

[48] Tony L, Schmitz. K Scott, Smith. Kevin S, Smith, "Machining Dynamics - Frequency Response to Improved Productivity", ISBN 978-0-387-09644-5, Chapter 4, Page 150-159, 2009.

[49] Product of the Tongtai Machine & Tool Co. Ltd., <https://www.tongtai.com.tw/en/product-detail.php?id=26>, Online accessed 20 May 2021.

[50] Product of the Yeong Chin Machinery Industries Co. Ltd., Machine & Tool Co. Ltd., <https://www.ycmcnc.com/>, and [https://www.techspex.com/machining-centers/ycm\(2460\)/5003](https://www.techspex.com/machining-centers/ycm(2460)/5003), Online accessed 12 September 2021.

[51] Product of the Precision Machinery Research & Development Center, <https://www.pmc.org.tw/>, Online accessed 20 May 2021

[52] Benardos, P. G., & Vosniakos, G, "Predicting surface roughness in machining: a review", International Journal of Machine Tools and Manufacture, 6:43(8):833-844, 2003. [https://doi.org/10.1016/S0890-6955\(03\)00059-2](https://doi.org/10.1016/S0890-6955(03)00059-2)

[53] BS EN ISO 4287:1997, "Geometrical product specification (GPS). Surface texture. Profile method. Terms, definitions, and surface texture parameters", STANDARD by British Standard / European Standard / International Organization for Standardization.


[54] Mitutoyo, "Portable Surface Roughness Tester - SURFTEST SJ-410 Series", [https://www.mitutoyo.com/wp-content/uploads/2013/02/2110\\_SJ-410.pdf](https://www.mitutoyo.com/wp-content/uploads/2013/02/2110_SJ-410.pdf), Online accessed 20 May 2021.

[55] Serope Kalpakjian, and Steven R. Schmid, "Manufacturing Engineering and Technology", Sixth Edition in SI Units, Prentice Hall, 2009, Chapter 23, Page 636.

---

**Publisher:** Chinese Institute of Automation Engineers (CIAE)

**ISSN:** 2223-9766 (Online)

 **Copyright:** The Author(s). This is an open access article distributed under the terms of the [Creative Commons Attribution License \(CC BY 4.0\)](https://creativecommons.org/licenses/by/4.0/), which permits unrestricted use, distribution, and reproduction in any medium, provided the original author and source are cited.

## Appendix A

### Symbols

$d$	Diameter of the tool [mm]
$r$	Radius of the tool [mm]
$N_t$	Number of flutes on the tool
$\beta$	Helix angle on the tool [deg]
$f_t$	Feed per tooth [mm/tooth]
$A_p$	Full axial depth of cut [mm]
$dz$	Differential axial depth of cut [mm]
$A_e$	The cutting width [mm]
$K_{tc}$	Tangential shearing force coefficient [N/mm <sup>2</sup> ]
$K_{rc}$	Radial shearing force coefficient [N/mm <sup>2</sup> ]
$K_{ac}$	Axial shearing force coefficient [N/mm <sup>2</sup> ]
$K_{te}$	Tangential edge force coefficient [N/mm]
$K_{re}$	Radial edge force coefficient [N/mm]
$K_{ae}$	Axial edge force coefficient [N/mm]
$b_{lim}$	The chatter-free axial depth of cut – critical depth of cut
$S$	Spindle Speed (rpm)
$f_c$	Chatter frequency.
$\varepsilon$	Phase between current and previous tool vibrations.
$K_s$	Force produced in cutting is proportional to all areas of the chip through this coefficient
$K_n$	The average directional factors depend on the radial cutting constant
$F_t$	Tangential cutting force [N]
$F_n$	Normal cutting force [N]
$F_a$	Axial cutting force [N]
$\bar{F}_x$	Average cutting force in the feed direction [N]
$\bar{F}_{xc}$	The slope of the linear model force in the feed direction [N]
$\bar{F}_{xe}$	The intercept of the linear model force in the feed direction [N]
$\bar{F}_y$	Average cutting force in the normal direction [N]
$\bar{F}_{yc}$	The slope of the linear model force in the normal direction [N]
$\bar{F}_{ye}$	The intercept of the linear model force in the normal direction [N]
$\bar{F}_z$	Average cutting force in the axial direction [N]
$\bar{F}_{zc}$	The slope of the linear model force in the axial direction [N]
$\bar{F}_{ze}$	The intercept of the linear model force in the axial direction [N]
$\theta$	Angle between feed and x-direction [deg]
$F_x$	Cutting force in x-direction [N]
$F_y$	Cutting force in y-direction [N]
$F_z$	Cutting force in z-direction [N]
$\emptyset$	The tool rotation angle in the helical flat end mill
$\emptyset_t$	The tool rotation angle at time t
$\emptyset_{st}$	Start angles
$\emptyset_{ex}$	Exit angles
$\emptyset_a$	Tooth angle or tool movement angle
$\tau$	The tooth passing periods in seconds.
$h(t)$	The dynamic chip thickness at time t
$\chi$	The angular delay (rad)
$\alpha_{xx}, \alpha_{yy}$	The direct transfer functions in the x and y direction
$\alpha_{xy}, \alpha_{yx}$	The cross-transfer functions
$[A_{r,i}]$	The Fourier coefficients
$n(t)$	Vibration of the current normal direction
$n(t - \tau)$	Vibration of the previous tooth at the current normal direction
$\omega_c$	The chatter frequencies (rad/s)
$FRF_{xx}$	The frequency respond function in x direction
$FRF_{yy}$	The frequency respond function in y direction
$FRF_{or}$	The oriented frequency respond function



A1. The solution of Chatter Stability in Milling

Altintas and Budak proposed zero-order analytical prediction of SLD [7], where the number of harmonics  $r' = 0$  for its Fourier coefficients  $[A_{r'}]$ . The average component of the Fourier series expansion is

$$[A_0] = \frac{1}{2\pi} \int_0^{2\pi} [A(\phi)] d\phi = \frac{1}{2\pi} \int_{\phi_{st}}^{\phi_{ex}} [A(\phi)] d\phi = \frac{N_t}{2\pi} \begin{bmatrix} \alpha_{xx} & \alpha_{xy} \\ \alpha_{yx} & \alpha_{yy} \end{bmatrix} \tag{1}$$

where  $[A]$  matrix entries [7] are the “time-varying directional dynamic force coefficients”.

$$\alpha_{xx} = \frac{1}{2} [\cos(2\phi) - 2K_n\phi + K_n \sin(2\phi)] \Big|_{\phi_{st}}^{\phi_{ex}} \tag{2}$$

$$\alpha_{xy} = \frac{1}{2} [-\sin(2\phi) - 2\phi + K_n \cos(2\phi)] \Big|_{\phi_{st}}^{\phi_{ex}} \tag{3}$$

$$\alpha_{yx} = \frac{1}{2} [-\sin(2\phi) + 2\phi + K_n \cos(2\phi)] \Big|_{\phi_{st}}^{\phi_{ex}} \tag{4}$$

$$\alpha_{yy} = \frac{1}{2} [-\cos(2\phi) - 2K_n\phi - K_n \sin(2\phi)] \Big|_{\phi_{st}}^{\phi_{ex}} \tag{5}$$

The average directional factors depend on the radial cutting constant  $K_n$  and the width of cut bound by entry ( $\phi_{st}$ ) and exit ( $\phi_{ex}$ ) angles. The dynamic milling equation according to [7] is:

$$\begin{pmatrix} F_x \\ F_y \end{pmatrix} e^{i\omega_c\tau} = \frac{1}{2} A_P K_{tc} [A_0] (1 - e^{i\omega_c\tau}) \begin{bmatrix} FRF_{xx} & 0 \\ 0 & FRF_{yy} \end{bmatrix} \begin{pmatrix} F_x \\ F_y \end{pmatrix} e^{i\omega_c\tau} \tag{6}$$

Rearranging Equation (23) gives

$$\begin{pmatrix} F_x \\ F_y \end{pmatrix} e^{i\omega_c\tau} \left( [I] - \frac{1}{2} A_P K_{tc} [A_0] (1 - e^{i\omega_c\tau}) \begin{bmatrix} FRF_{xx} & 0 \\ 0 & FRF_{yy} \end{bmatrix} \right) = 0 \tag{7}$$

Which has a non-trivial solution only if

$$\det \left( [I] - \frac{1}{2} A_P K_{tc} [A_0] (1 - e^{i\omega_c\tau}) \begin{bmatrix} FRF_{xx} & 0 \\ 0 & FRF_{yy} \end{bmatrix} \right) = 0 \tag{8}$$

Where  $[I] = \begin{bmatrix} 1 & 0 \\ 0 & 1 \end{bmatrix}$  is the 2x2 identity matrix.  $\begin{bmatrix} FRF_{xx} & 0 \\ 0 & FRF_{yy} \end{bmatrix} = [FRF]$ . The product  $[A_0] [FRF]$  from Equation (25) is analogous to the oriented FRF. Expanding it gives Equation (26)

$$\begin{aligned} [A_0][FRF] &= \frac{N_t}{2\pi} \begin{bmatrix} \alpha_{xx} & \alpha_{xy} \\ \alpha_{yx} & \alpha_{yy} \end{bmatrix} \begin{bmatrix} FRF_{xx} & 0 \\ 0 & FRF_{yy} \end{bmatrix} \\ &= \frac{N_t}{2\pi} \begin{bmatrix} \alpha_{xx}FRF_{xx} & \alpha_{xy}FRF_{yy} \\ \alpha_{yx}FRF_{xx} & \alpha_{yy}FRF_{yy} \end{bmatrix} = \frac{N_t}{2\pi} [FRF_{or}] \end{aligned} \tag{9}$$

The characteristic Equation can be rewritten as shown in Equation (27)

$$\det([I] + \forall [FRF_{or}]) = 0 \tag{10}$$

where  $\forall$  is a new variable,

$$\forall = -\frac{N_t}{4\pi} A_P K_{tc} (1 - e^{-i\omega_c\tau}) \tag{11}$$

The characteristic Equation becomes just a quadratic function as shown in Equation (29)

$$a_0 \forall^2 + a_1 \forall + 1 = 0 \tag{12}$$

Where  $a_0 = FRF_{xx}FRF_{yy}(\alpha_{xx}\alpha_{yy} - \alpha_{xy}\alpha_{yx})$  and  $a_1 = \alpha_{xx}FRF_{xx} + \alpha_{yy}FRF_{yy}$

The two roots are the system eigenvalues,  $\forall_1$  and  $\forall_2$  shown in Equation (30)

$$\forall_{1,2} = -\frac{1}{2a_0} (a_1 \mp \sqrt{a_1^2 - 4a_0}) \tag{13}$$

Equation (28) can be rewritten by recognizing the complex nature of the eigenvalues,  $\forall = \forall_{Re} + i\forall_{Im}$  and substituting the Euler identity  $e^{-i\omega_c\tau} = \cos(\omega_c\tau) - i \sin(\omega_c\tau)$

$$\forall_{Re} + i\forall_{Im} = -\frac{N_t}{4\pi} A_P K_{tc} \{1 - [\cos(\omega_c\tau) - i \sin(\omega_c\tau)]\} \tag{14}$$

Equation (31) is solved for  $A_P$  to obtain the chatter-free axial depth of cut (critical depth of cut),  $b_{lim}$ :

$$b_{lim} = -(\forall_{Re} + i\forall_{Im}) \frac{4\pi}{N_t K_{tc}} \frac{l}{\{1 - [\cos(\omega_c\tau) - i \sin(\omega_c\tau)]\}} \tag{15}$$

$$b_{lim} = -\frac{2\pi}{N_t K_{tc}} \left( \frac{(\forall_{Re}(1 - \cos(\omega_c\tau)) + \forall_{Im}\sin(\omega_c\tau))}{(1 - \cos(\omega_c\tau))} + i \frac{(\forall_{Im}(1 - \cos(\omega_c\tau)) - \forall_{Re}\sin(\omega_c\tau))}{(1 - \cos(\omega_c\tau))} \right) \tag{16}$$

Because  $b_{lim}$  must be a real-value, the imaginary part of Equation (33) is equal to zero.

$$\forall_{Im}(1 - \cos(\omega_c\tau)) - \forall_{Re}\sin(\omega_c\tau) = 0 \tag{17}$$

Set the new variable

$$\exists = \frac{\forall_{Im}}{\forall_{Re}} = \frac{\sin(\omega_c\tau)}{1 - \cos(\omega_c\tau)} \tag{18}$$

Equation (33) is now rewritten to obtain the final expression for the critical axial depth of cut

$$b_{lim} = -\frac{2\pi}{N_t K_{tc}} \forall_{Re} (1 + \exists^2) \tag{19}$$

The eigenvalue problem as stated in Equation (27),  $\det([I] + \forall[FRF_{or}]) = 0$ , can be rewritten in the traditional format required by the formula  $\det([FRF_{or}] - \lambda[I]) = 0$ , where the new eigenvalue expression is  $\lambda = \frac{4\pi}{N_t} \frac{1}{A_p K_{tc}(1-e^{-i\omega_c\tau})}$

$$\lambda = \lambda_{Re} + i\lambda_{Im} = \frac{4\pi}{N_t} \frac{1}{A_p K_{tc}(1-e^{-i\omega_c\tau})} \tag{20}$$

Equation (37) is solved for  $A_p$  to obtain the chatter-free axial depth of cut (critical depth of cut),  $\widetilde{b}_{lum}$ , as is expressed in Eq. (38):

$$\widetilde{b}_{lum} = \frac{4\pi}{N_t K_{tc}(\lambda_{Re} + i\lambda_{Im})(1 - [\cos(\omega_c\tau) + i \sin(\omega_c\tau)])}$$

$$\widetilde{b}_{lum} = \frac{2\pi(\lambda_{Re} - i\lambda_{Im})(1 - [\cos(\omega_c\tau) - i \sin(\omega_c\tau)])}{N_t K_{tc}(\lambda_{Re}^2 + \lambda_{Im}^2)(1 - \cos(\omega_c\tau))} \tag{21}$$

$$\widetilde{b}_{lum} = \frac{2\pi}{N_t K_{tc}(\lambda_{Re}^2 + \lambda_{Im}^2)} \left[ \frac{\lambda_{Re}(1 - \cos(\omega_c\tau)) - \lambda_{Im}\sin(\omega_c\tau)}{(1 - \cos(\omega_c\tau))} + i \frac{-\lambda_{Im}(1 - \cos(\omega_c\tau)) - \lambda_{Re}\sin(\omega_c\tau)}{(1 - \cos(\omega_c\tau))} \right]$$

Because  $\widetilde{b}_{lum}$  must be a real-value, the imaginary part of Equation (38) is equal to zero.

$$-\lambda_{Im}(1 - \cos(\omega_c\tau)) - \lambda_{Re}\sin(\omega_c\tau) = 0 \tag{22}$$

Set the new variable

$$K = \frac{\lambda_{Im}}{\lambda_{Re}} = -\frac{\sin(\omega_c\tau)}{1 - \cos(\omega_c\tau)} \tag{23}$$

The corresponding revised stability limit becomes:

$$\widetilde{b}_{lum} = \frac{2\pi}{N_t K_{tc}(\lambda_{Re}^2 + \lambda_{Im}^2)} \lambda_{Re}(1 + K^2) \tag{24}$$

Where  $K = \frac{\lambda_{Im}}{\lambda_{Re}}$  and the spindle speed equations are also modified to be

$$\tau = \frac{1}{\omega_c} (\varepsilon + j \times 2\pi) \text{ (s)} \tag{25}$$

$$\varepsilon = \pi - 2\psi \text{ (rad)}, \psi = \tan^{-1}(K) \text{ (rad)},$$

$$\text{and } S = \frac{60}{N_t\tau} \text{ (rpm)} \tag{26}$$

Where  $j$  is the integer number of full vibration waves. The stability lobe diagram is obtained by plotting  $\widetilde{b}_{lum}$  versus  $S$  for each chatter frequency (the minimum at each spindle speed is selected to define the stability boundary).

A2. Identification of cutting force coefficients in helical flat end mill in all case is shown in Table A-1

**Table A-1** Calculation of cutting force coefficients (CFCs) in all case

CFCs	Half – up milling	Half – down milling	Slotting	Eqn
$K_{rc}$	$-\left(\frac{2\overline{F}_{yc}}{\pi} + \overline{F}_{xc}\right) / \left(\frac{N_t A_p}{8} + \frac{N_t A_p}{2\pi^2}\right)$	$\frac{4\pi}{N_t A_p} \left(\overline{F}_{yc} - \frac{N_t A_p}{8} K_{tc}\right)$	$\frac{-4\overline{F}_{xc}}{N_t A_p}$	(27)
$K_{tc}$	$-\frac{4\pi}{N_t A_p} \left(\overline{F}_{xc} + \frac{N_t A_p}{8} K_{rc}\right)$	$\left(\frac{2\overline{F}_{xc}}{\pi} + \overline{F}_{yc}\right) / \left(\frac{N_t A_p}{8} + \frac{N_t A_p}{2\pi^2}\right)$	$\frac{4\overline{F}_{yc}}{N_t A_p}$	(28)
$K_{re}$	$\frac{-\pi(\overline{F}_{xe} + \overline{F}_{ye})}{N_t A_p}$	$\frac{2\pi}{N_t A_p} \left(\overline{F}_{ye} - \frac{N_t A_p}{2\pi} K_{te}\right)$	$\frac{-\pi\overline{F}_{xe}}{N_t A_p}$	(29)
$K_{te}$	$-\frac{2\pi}{N_t A_p} \left(\overline{F}_{xe} + \frac{N_t A_p}{2\pi} K_{re}\right)$	$\frac{\pi(\overline{F}_{xe} + \overline{F}_{ye})}{N_t A_p}$	$\frac{\pi\overline{F}_{ye}}{N_t A_p}$	(30)
$K_{ac}$	$\frac{2\pi\overline{F}_{zc}}{N_t A_p}$	$\frac{2\pi\overline{F}_{zc}}{N_t A_p}$	$\frac{\pi\overline{F}_{zc}}{N_t A_p}$	(31)
$K_{ae}$	$\frac{4\overline{F}_{ze}}{N_t A_p}$	$\frac{4\overline{F}_{ze}}{N_t A_p}$	$\frac{2\overline{F}_{ze}}{N_t A_p}$	(32)